PHASE TRANSITIONS INDUCED BY FEMTOSECOND PULSES

E. N. Glezer, L. Huang, Y. Siegal, J. P. Callan, and E. Mazur

Division of Applied Sciences and Department of Physics, Harvard University, Cambridge, MA 02138

ABSTRACT

Optical studies of semiconductors under intense femtosecond laser pulse excitation suggest that an ultrafast phase transition takes places before the electronic system has time to thermally equilibrate with the lattice. The excitation of a critical density of valence band electrons destabilizes the covalent bonding in the crystal, resulting in a structural phase transition. The deformation of the lattice leads to a decrease in the average bonding-antibonding splitting and a collapse of the band-gap. Direct optical measurements of the dielectric constant and second-order nonlinear susceptibility are used to determine the time evolution of the phase transition.

INTRODUCTION

Intense, femtosecond laser-pulse excitation of semiconductors provides a unique opportunity for observing the dynamics of a phase transition. The semiconductor-metal transition that can result from such excitation[1-11] is particularly interesting because it illustrates the critical role high free-carrier densities can play in modifying the electronic and structural properties of semiconductors. Understanding the complex dynamics involved in laser-induced phase transitions requires an explicit determination of the behavior of intrinsic material properties during these transitions.

Dielectric Constant

Without direct determination of the time-evolution of the dielectric constant, interpretation of reflectivity and second-harmonic data has relied to date on making assumptions about the functional form of the dielectric constant. Specifically, it has been assumed that the changes in the dielectric constant induced by the excitation are dominated by the free carrier contribution to the optical susceptibility. Under this assumption, the changes in the dielectric constant have been modeled using a Drude-model formalism.[1, 7, 12] While this type of assumption is legitimate at lower excitation regimes, it is misleading in the case of laser-induced disordering experiments. Misinterpretation of the data arises because a single-incident-angle reflectivity value does not correspond to a unique value of the dielectric constant. Thus, one can reproduce single-incident-angle reflectivity data using dielectric constant values that are completely different from the actual ones.

To avoid relying on an assumed functional form for the dielectric constant in interpreting the results of femtosecond pump-probe experiments on GaAs, we directly determined the time evolution of the real and imaginary parts of the dielectric constant. Specifically, we experimentally determined the behavior of the complex dielectric constant at photon energies of 2.2 eV and 4.4 eV following excitation with an intense, 70-fs pump pulse at 1.9 eV. To uniquely extract the real and imaginary parts of the dielectric constant, two independent measured quantities are necessary. Therefore, at each probe frequency we measured the *p*-polarized reflectivity at two carefully chosen angles of incidence using two simultaneous 70-fs probe beams.[8-10] We then converted each measured pair of reflectivities to the corresponding complex value of the dielectric constant as a function of pump-probe time delay. We verified that our two-angle technique yielded dielectric constant values consistent with reflectivity measurements at a third angle of incidence. The general approach of employing multiparameter optical probing to distinguish Drude and interband contributions to the dielectric constant has been used in other recent work, using ellipsometric techniques.[13-16] The data we present in this paper show that for excitation fluences greater than 0.5 kJ/m^2, the Drude model does not adequately describe the induced changes to the dielectric constant. The results indicate that changes in the interband transition contribution to the optical susceptibility dominate the behavior of the dielectric constant, as opposed to changes in the free carrier contribution as has been generally assumed. This finding implies that the previously observed initial reflectivity rise following high-intensity femtosecond laser-pulse excitation of semiconductors[1, 3, 5-7] is due to large changes in the electronic band structure which result from the excitation.

Second-Order Susceptibility

Because of its sensitivity to crystal symmetry, second-harmonic generation has been used by a number of researchers to study laser-induced phase transitions in semiconductors.[3-7, 17-19] The sensitivity of second-harmonic generation to the symmetry properties of a nonlinear crystal arises from the dependence of second-harmonic generation on the material's second-order optical susceptibility $\chi^{(2)}$, which reflects the symmetry group of the crystal.[20] A change in the material's symmetry properties, such as may occur in a phase transition, affects $\chi^{(2)}$ and results in a change in the detected second-harmonic signal. However, the detected second-harmonic signal depends on more material properties than just $\chi^{(2)}$. In particular, it depends also on the values of the linear optical susceptibility $\chi^{(1)}$ (or, equivalently, the linear dielectric constant ε) at both the fundamental frequency ω and the second-harmonic frequency 2ω of the probe beam used for second-harmonic generation.[20] Thus, to extract the behavior of $\chi^{(2)}$ from second-harmonic generation measurements, one must first know the behavior of $\varepsilon(\omega)$ and $\varepsilon(2\omega)$.

We combined experimental measurements of $\varepsilon(\omega)$ and $\varepsilon(2\omega)$ following intense femtosecond laser-pulse excitation of GaAs[8-11] with second-harmonic generation measurements under identical excitation conditions to unambiguously determine the response of $\chi^{(2)}$ to this type of excitation. This experiment is unique because the response of $\chi^{(2)}$ to femtosecond laser-pulse excitation is extracted from second-harmonic generation measurements by explicitly taking into account the experimentally determined response of $\chi^{(1)}$ to the same excitation rather than by assuming that the effect of $\chi^{(1)}$ on the second-harmonic generation measurements is small. In fact, the experimentally-determined changes in $\chi^{(1)}$ are much larger than expected,[8-11] and our results show that these changes have a significant effect on the detected second-harmonic signal, contrary to earlier assumptions.[3, 5, 7] This effect masks the behavior of $\chi^{(2)}$ at fluences below 0.6 kJ/m^2, as will be discussed later in this paper. Expressly incorporating the changes in the dielectric constant in this experiment has uncovered previously unobserved behavior in this fluence range marked by recovery of $\chi^{(2)}$ to its initial value on a picosecond time scale.

Optical Properties and Electronic Structure

The interband transition contribution $\chi_{\text{interband}}(\omega)$ to the dielectric function arises from the coupling of states in different bands through the applied electric field. In a direct-gap semiconductor like GaAs, $\chi_{\text{interband}}(\omega)$ is dominated by direct, or vertical, transitions and is therefore closely related to the joint density of states $J(\omega)$ of the material. The joint density of states, in turn, is directly determined by the electronic band structure:[21, 22]

$$J(\omega) = \sum_{v,c} \frac{2}{(2\pi)^3} \int d^3k \quad \delta\left[\omega_{vc}(\mathbf{k}) - \omega\right], \tag{1}$$

where v and c are respectively valence and conduction band indices, $\hbar\omega_{vc}$ is the energy separation between band v and band c at a crystal momentum value of $\mathbf{k}$, and the integral is over the Brillouin zone. In the ground state (valence band filled and conduction band empty), the imaginary part of $\chi_{\text{interband}}(\omega)$ approximately satisfies the relation[21, 22]

$$\text{Im}[\chi_{interband}(\omega)] \propto \frac{1}{\omega^2} J(\omega), \tag{2}$$

illustrating the connection between the electronic band structure and the interband transition contribution to the dielectric constant.

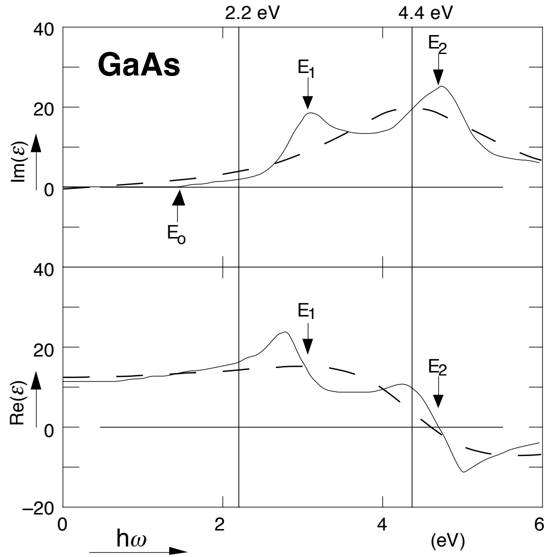

Fig. 1 Dielectric function of GaAs. The solid curves show the dielectric function taken from the literature (see Ref. 19). E_o labels the fundamental absorption edge, corresponding to the minimum band gap while E_1 and E_2 label the two main absorption peaks. The dashed curves show a fit of the single-oscillator dielectric function to the solid curves.

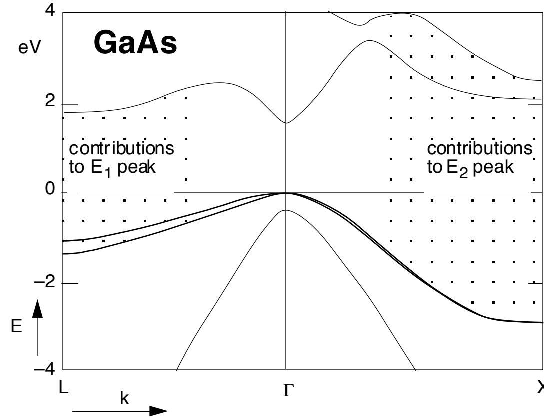

Fig. 2 A section of the electronic band structure of GaAs (see Ref. 17) showing some of the regions that contribute to the E_1 and E_2 absorption peaks in the dielectric function.

Most Group IV and III-V semiconductors have qualitatively similar joint densities of states, leading to similar dielectric functions in the ground state.[21-23] The solid curves in Fig. 1 show both the real and imaginary parts of the dielectric function of undoped GaAs at room temperature.[24] The three main features labeled E_o, E_1, and E_2 are common to the Group IV and III-V semiconductors although their locations and the relative sizes of these features vary from material to material. The point E_o (at 1.4 eV for GaAs) marks the fundamental band edge below which Im(ε) is zero; E_1 and E_2, (located at 3.0 eV and 4.75 eV, respectively, for GaAs[25]) label the two main absorption peaks in the spectrum. These peaks arise from regions in the band structure (the region around the L-point for the E_1 peak and the region around the X-point for the E_2 peak — see GaAs band structure diagram in Fig. 2) in which the valence band is roughly parallel to the conduction band, resulting in a large joint density of states for direct interband transitions.[21] The E_2 peak, which is roughly coincident with the zero-crossing in Re(ε), is the stronger of the two absorption peaks, and its location approximately gives the value of the average bonding-antibonding splitting of GaAs.[22]

In the simplest approximation, the overall shape of the GaAs dielectric function (the solid curves in Fig. 1) resembles that of a charged particle in a damped harmonic oscillator potential. We can model the GaAs dielectric function as a single average harmonic oscillator with a resonant frequency

that corresponds to the average bonding-antibonding splitting,[21] and a width that is related to the spectral range over which the joint density of states is large. The dashed curves in Fig. 1 represent a fit of the single-oscillator dielectric function[26] to the ground-state dielectric function of GaAs. While this type of picture does not describe the structure in the semiconductor dielectric function in detail, it provides a simple physical interpretation for the overall shape and highlights some important characteristics. In particular, it illustrates that the main interband absorption peak in the semiconductor dielectric function has the same features as an oscillator resonance: a zero-crossing in the real part coinciding with a peak in the imaginary part. This simplified picture will be helpful in the interpretation of the data presented below.

As evidenced by changes observed in the reflectivity, excitation of a semiconductor with a laser pulse modifies the dielectric constant of the material.[2, 3, 5, 12, 17, 18, 27, 28] The model generally used for the time-dependent dielectric function $\varepsilon(\omega,t)$ of a semiconductor following laser-pulse excitation involves the assumption that the interband contribution to the susceptibility does not change significantly as a result of the excitation: $\chi_{\text{interband}}(\omega,t) \approx \chi_{\text{interband}}(\omega)$.[1, 29] Instead, changes in the dielectric function are attributed mainly to the time dependence of $\chi_{\text{Drude}}(\omega,t)$ arising from the time-dependent free-carrier density $N(t)$ produced by the excitation. The free carrier contribution to the dielectric constant of a semiconductor is generally treated in the framework of the Drude model for the ac conductivity of free electrons.[12, 30, 31] For a semiconductor with a conduction-band electron density of N_e and a valence-band hole density of N_h, the Drude contribution of the free carriers to the optical susceptibility is given by

$$\chi_{\text{Drude}}(\omega) = \frac{ie^2}{\omega}\left[\frac{N_e\tau_e}{m_e^*(1-i\omega\tau_e)} + \frac{N_h\tau_h}{m_h^*(1-i\omega\tau_h)}\right], \tag{3}$$

where e is the charge of the electron, and $m_{e,h}^*$ and $\tau_{e,h}$ are the effective mass and mean collision time of the free electrons and holes. If the free carriers are produced by optical excitation, then $N_e = N_h = N$, where N is the number of electron-hole pairs created by the excitation.

The free-carrier density $N(t)$ created by the laser-pulse excitation depends on the excitation fluence ϕ. At a fixed time t after the excitation, $N(\phi, t)$ increases monotonically with excitation fluence. Based on this model, one would expect $\text{Re}[\varepsilon(\omega, \phi, t)]$ to decrease monotonically and $\text{Im}[\varepsilon(\omega, \phi, t)]$ to increase monotonically with increasing excitation fluence. Furthermore, with $\omega\tau >> 1$, the increase in $\text{Im}[\varepsilon(\omega, \phi, t)]$ should be only slight.

While this Drude-like model for the dielectric constant of a laser-excited semiconductor adequately describes data at low and moderate carrier excitation levels ($N \leq 10^{20}\ \text{cm}^{-3}$),[13, 32] the data we present below show that it cannot be used to analyze reflectivity data at high carrier excitation levels ($N \geq 10^{21}\ \text{cm}^{-3}$). Our experimental results indicate that, in this strong excitation regime, the response of the dielectric function to the laser pulse excitation is dominated by changes in the interband transition

contribution to the dielectric constant resulting from a major alteration of the electronic band structure. The difference between the expected behavior of $\varepsilon(\omega,\phi,t)$ based on previous assumptions and the experimentally observed behavior is highlighted in the results section.

EXPERIMENTS

The results presented in this paper involve three sets of measurements made using a two-color pump-probe technique. The dielectric constant data were taken using a 70-fs, 1.9-eV (635-nm) pump beam and a simultaneous pair of 70-fs, 2.2-eV (570-nm) probe beams and also using the same pump beam conditions but a doubled probe photon energy of 4.4 eV (285 nm). The second-harmonic data were taken with the same pump conditions and a single 2.2-eV probe beam. To generate pump and probe beams at different frequencies, we pass the amplified output of a colliding pulse modelocked laser through a 20-mm, single-mode, polarization-preserving optical fiber.[33] Self-phase modulation in the fiber broadens the spectrum of the input pulse from 5 to 200 nm. By splitting this continuum beam with a broadband beamsplitter, we can independently amplify different spectral regions within the 200-nm bandwidth using two separate amplifier chains.[34] A three-stage amplifier using the dye DCM produces a 300-μJ pump beam centered at 635 nm with a 20-nm bandwidth; a two-stage amplifier using the dye Rhodamine 6G produces a 30-μJ probe beam centered at 570 nm with a 10-nm bandwidth. Both amplifiers are pumped by a frequency-doubled, 10-Hz Nd:YAG laser. Following amplification, each beam is compressed by a separate grating pair to a 70-fs pulse width (FWHM).

To determine both the real and imaginary parts of the dielectric constant of GaAs with femtosecond time resolution, we simultaneously measure the reflectivity at two different angles of incidence as a function of pump-probe time delay.[34] In the 2.2-eV experiment, the pair of probe beams is produced simply by splitting the 570-nm beam in two. In the 4.4-eV experiment, we first double the 570-nm beam in a 100-μm thick BBO crystal before splitting the beam. The probing geometries for both experiments are summarized in Fig. 3. In both cases, the incident beams are polarized in the plane of incidence and are focused onto the same spot on an insulating (110) GaAs wafer (Cr doped, $\rho > 7\times10^{7}\ \Omega$ cm), which is exposed to air. To monitor a uniformly excited region, we focus the probe beams more tightly than the pump beam: the probed surface area is about 16 times smaller than the 0.01-mm^2 focal area of the pump beam on the sample. Uniform excitation in the probed region is further assured by the smaller penetration depth of the probe beams (between 5 and 170 nm at 2.2 eV and 5 and 10 nm at 4.4 eV)[35] compared to that of the pump beam (270 nm). The pump pulse fluence at each pump-probe time delay spans a range from 0 to 2.5 kJ/m^2. The probe beam fluence never exceeds 0.1 kJ/m^2 so as not to produce any detectable changes in the dielectric constant. To avoid cumulative damage effects, we translate the sample

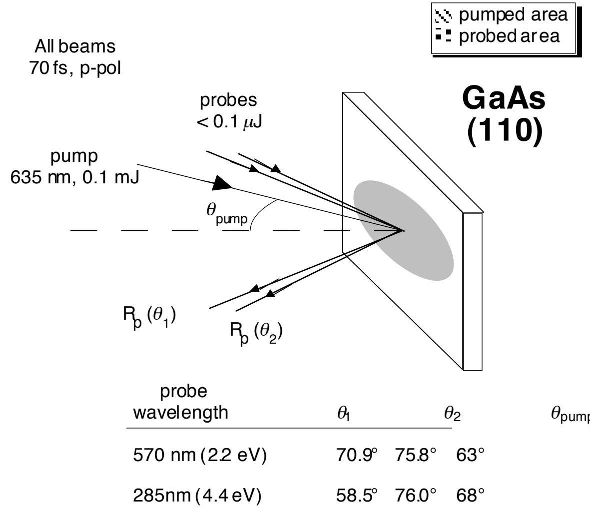

Fig. 3 Probing geometry and incident angles for the 2.2-eV and 4.4-eV measurements. All beams are *p*-polarized.

during data collection so that each data point is obtained at a new spot on the sample.

We convert each pair of reflectivity measurements to the corresponding real and imaginary parts of the dielectric constant by numerically inverting the Fresnel formula for reflectivity as a function of incident angle. Setting one of the probe beam angles of incidence to the Brewster angle provides good sensitivity in distinguishing changes in $\mathrm{Re}(\varepsilon)$ from changes in $\mathrm{Im}(\varepsilon)$ because the *p*-polarized reflectivity at this angle is determined mainly by $\mathrm{Im}(\varepsilon)$.[36] We base our choice of the second incident angle, which is not as critical, on constraints in the experimental setup. The two angles of incidence for the 2.2-eV measurements were 75.8° and 70.9°; in the 4.4-eV measurements we used 76.0° and 58.5°. To keep the angular separation between pump and probes small, we used a 63° incident angle for the *p*-polarized pump beam in the 2.2-eV experiment and a 68° incident angle in the 4.4-eV experiment.

Because the GaAs surface oxidizes in air, we use a three-phase model (air-oxide-GaAs) in converting the reflectivity data to values for the dielectric constant. Surface roughness effects can be accounted for in this model by adjusting the effective thickness of the oxide layer.[37] We calibrated the effective thickness of the oxide layer by measuring reflectivity as a function of incident angle in the absence of excitation by a pump pulse. Using the ground-state dielectric constant of GaAs[24] and a value of $\varepsilon = 4$ for the dielectric constant of the oxide layer,[37] we fit the three-phase model to the measured angle dependence with the effective oxide layer thickness as a fit parameter. This procedure consistently yielded an effective thickness for the oxide layer of about 4 nm. In the 2.2-eV experiment the obtained value was 4.2 ± 0.4 nm while in the 4.4-eV experiment the value was 4.4 ± 0.4 nm.

As a consistency check of our determination of the dielectric constant, we measured the time-evolution of the reflectivity at a third, completely

different, angle of incidence (45° for the 2.2-eV case and 35.5° for the 4.4-eV case) under similar pump pulse excitation conditions at both probe frequencies. We then calculated the expected reflectivity at that third incident angle using our experimentally determined time- and fluence-dependent values for the dielectric constant. The measured reflectivity showed excellent agreement with the calculated reflectivity at this third angle of incidence for both the 2.2-eV and 4.4-eV data. An example of this consistency check is shown in the results section (see Fig. 7).

In the second-harmonic generation (SHG) measurements the pump beam arrives at an incident angle of 63° with respect to the surface normal while the probe beam comes in with an incident angle of 45°. Both beams are polarized in the plane of incidence. The (100) sample surface is set to a position with two of the crystallographic axes in the plane of incidence of the beams and the third one perpendicular to it. To monitor a uniformly excited region, we again focus the probe beams more tightly than the pump beam. Uniform excitation in the probed region is further assured by the small absorption depth of the second-harmonic radiation generated in the sample (about 20 nm) compared to that of the pump beam (270 nm). The pump pulse fluence at each pump-probe time delay is varied over a range from 0 to 2.0 kJ/m^2.

To extract the behavior of the second-order susceptibility we combine the measurements of the second-harmonic generation with the measurements of the dielectric constant, as described in the results section. We checked the consistency between the SHG data set and the 2.2 eV dielectric constant measurements by simultaneously measuring the linear reflectivity along with the second-harmonic signal. To this end, we used a dichroic beamsplitter to separate the second-harmonic radiation generated in reflection from the reflected fundamental radiation, measuring the second-harmonic signal using a photomultiplier tube and the fundamental signal with a calibrated phototube. The reflectivity values measured in this way agree with the reflectivity values we calculate for 45° incident angle and polarization in the plane of incidence using the measured dielectric constant, verifying that the excitation conditions and fluence calibrations for both sets of measurements are indeed identical.

RESULTS

Dielectric Constant at 2.2 eV

Figure 4 summarizes the experimental data on the dielectric constant at 2.2 eV. In Fig. 4a, Re(ε) (filled circles) and Im(ε) (open circles) are plotted vs. pump-probe time delay for four different excitation fluences; in Fig. 4b, Re(ε) and Im(ε) are plotted vs. pump fluence at four different time delays. The change induced in the dielectric constant by the pump pulse excitation is completely different from that expected from the free carrier contribution to the optical susceptibility. At pump fluences near 1 kJ/m^2, Im(ε) starts at an initial value of about 2, rises to a peak near 60, and then drops to somewhere between 10 and 15 — a strong contrast to the slight,

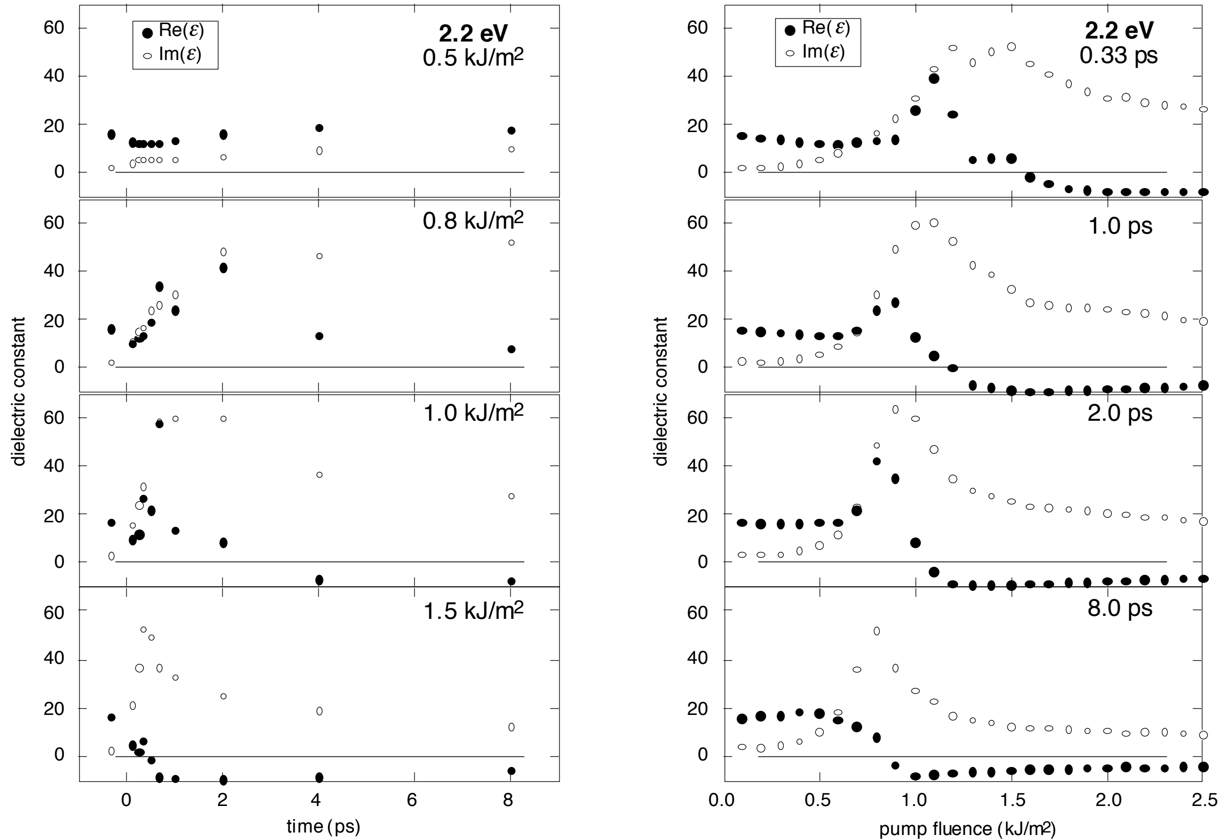

Fig. 4 a, b Dielectric constant at 2.2 eV vs. pump-probe time-delay for four different pump fluences and vs. pump fluence for four different time-delays. ●: Re(ε), ○: Im (ε).

featureless increase predicted by the Drude model. Re(ε), meanwhile, initially decreases slightly but then sharply increases before dropping through zero. Note that the zero-crossing of Re(ε) roughly coincides with the peak in Im(ε).

The results shown in Fig. 4 indicate that a strong absorption peak comes into resonance with the probe frequency as a result of the excitation. The resonance behavior is most striking in Fig. 4b because the features are particularly clear when plotted versus pump fluence. This behavior must result from an interband absorption peak and not from a free carrier plasma resonance because the zero-crossing in Re(ε) is accompanied by a peak in Im(ε) rather than by a steady increase. From the behavior of Re(ε), we can infer the time evolution of this interband absorption peak. Because Re(ε) is initially positive, the resonant frequency of the observed absorption peak evidently starts out higher than the probe frequency; it then sweeps down through the probe frequency as Re(ε) drops through zero.

The rate at which the resonant frequency of the absorption peak drops through the probe frequency depends on the strength of the excitation: the higher the pump fluence, the faster Re(ε) drops through zero. For fluences around 2.0 kJ/m^2, the absorption peak comes into resonance with the probe frequency within a few hundred femtoseconds; at fluences just

above 0.8 kJ/m^2, on the other hand, the absorption peak takes on the order of 10 picoseconds to come into resonance. For fluences below 0.8 kJ/m^2, Re(ε) never goes through zero, indicating that the excitation is not strong enough to bring the resonant frequency of the peak down to the probe frequency.

The threshold fluence for permanent damage to the sample is 1.0 kJ/m^2. We determined this threshold by correlating pump pulse fluence with the size of damage spots on the sample measured through a microscope. Above the damage threshold the pump pulse induces irreversible changes in the sample while below the damage threshold the induced changes are reversible. Measurements taken several seconds after the excitation confirm that the dielectric constant eventually returns to its initial value for fluences below the damage threshold. Note, however, that the absorption peak comes into resonance with the probe frequency even for pump fluences below this damage threshold.

The use of the Fresnel equations to extract the dielectric constant from reflectivity measurements presumes the existence of a sharp boundary between two different media. While this assumption is clearly justified below the damage threshold, at higher fluences density gradients can develop due to hydrodynamic expansion at the surface.[14] Furthermore, the hydrodynamic expansion can lead to the formation of an absorptive cloud, accompanied by non-specular scattering of the probe light. The formation of such an absorptive cloud has been seen in silicon, beginning at about 10 ps after excitation by a pulse with fluence about five times greater than the damage threshold.[2] In GaAs, a decrease in the specular reflectivity and the onset of non-specular scattering of the probe light, also beginning about 10 ps after the excitation, has been observed above the damage threshold.[28] To remain within the validity range of the sharp boundary assumption we limit the range of time delays over which we extract the dielectric constant to 8 ps. By measuring the reflectivity at a third angle for both 2.2 eV and 4.4 eV experiments we verified that the Fresnel equations are indeed valid over our entire experimental range.

Qualitative Picture — Bandgap Collapse

It is useful at this point to develop a qualitative interpretation of the data presented in the preceding section. The first step in interpreting the data is to attach a physical significance to the interband absorption peak. As discussed in the introduction, the dielectric function of GaAs can be approximated by that of a damped single harmonic oscillator with a resonant frequency equal to the average bonding-antibonding splitting.[21] Identifying the interband absorption peak in the data with the harmonic oscillator absorption peak, we can think of the shift in this peak as a drop in the average bonding-antibonding splitting. In GaAs, the average bonding-antibonding splitting in the ground state is about 4.75 eV.[22, 25] The 2.2-eV data then indicate that the laser-pulse excitation induces a drop in the average bonding-antibonding splitting from 4.75 eV to below 2.2 eV. Note that this drop in the average splitting by more than a factor of two occurs even for fluences below the damage threshold, an excitation regime in which the induced changes are *reversible*.

Figure 5 illustrates schematically the qualitative picture that emerges from the 2.2-eV data. The average bonding-antibonding splitting $\Delta E_{b\text{-}a}$ starts out far above 2.2 eV, so the probe photon energy lies at the foot of the single-oscillator absorption peak where Im(ε) is small (step 1 in Fig. 5). As a result of the excitation in step 1, $\Delta E_{b\text{-}a}$ begins to decrease, leading to a downward shift in the resonant frequency of the single-oscillator absorption peak and therefore a rise in Im(ε) at 2.2 eV (step 2 in Fig. 5).[35] As $\Delta E_{b\text{-}a}$ drops past 2.2 eV (step 3 in Fig. 5), Im(ε) goes through a peak. If

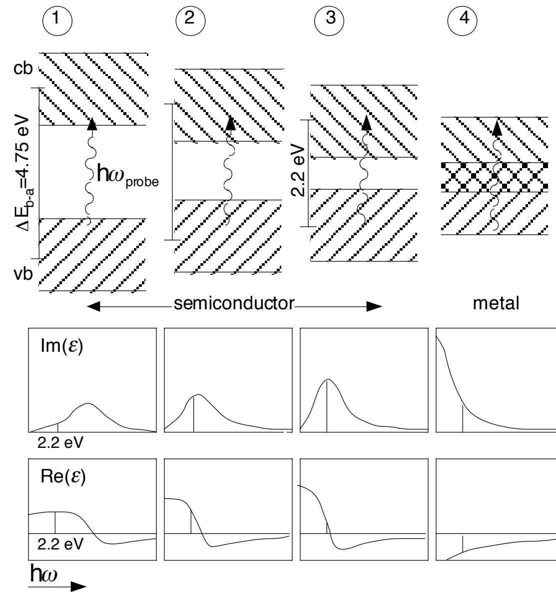

Fig. 5 Schematic representation of the bandgap collapse. The pump pulse leads to a drop in the average bonding-antibonding splitting from its initial value of about 4.75 eV to below the probe photon energy of 2.2 eV. If the minimum in the conduction band drops below the maximum in the valence band, the material takes on metallic properties. The drop in average bonding-antibonding splitting appears as a shift in the main absorption peak in the dielectric function, as illustrated in the figure. cb: conduction band; vb: valence band; $\Delta E_{b\text{-}a}$: average bonding-antibonding splitting; $h\omega_{probe}$: probe photon energy.

$\Delta E_{b\text{-}a}$ drops far enough, the minimum in the conduction band will drop below the maximum in the valence band and the semiconductor will take on metallic properties (step 4 in Fig. 5). The 2.2-eV dielectric constant at high fluences and long time delays, after the collapse of the bandgap, is consistent with the characteristics of a poor metal and is similar to that of liquid silicon[30] and liquid carbon[38] produced by laser pulse excitation.

This interpretation of the 2.2-eV data in terms of a drop in the average bonding-antibonding splitting allows us to predict qualitatively the behavior of the dielectric constant at different photon energies under similar excitation conditions. In particular, for a given excitation strength, the dielectric constant at a probe photon energy between 2.2 eV and 4.75 eV should exhibit resonance features at an earlier pump-probe time delay than the dielectric constant at 2.2 eV. Equivalently, for a fixed pump-probe time delay, the dielectric constant at a probe photon energy in the above range should exhibit resonance features at a lower pump fluence than the dielectric constant at 2.2 eV.

Dielectric Constant at 4.4 eV

To verify the interpretation described in the preceding section, we measured the behavior of the dielectric constant at 4.4 eV, which is only slightly below the initial value of the average bonding-antibonding splitting of GaAs. Figure 6 summarizes the data at 4.4 eV. Figure 6a presents the time-dependence of the 4.4-eV dielectric constant at the same four pump fluences shown in Fig. 4a, and Fig. 6b shows the fluence dependence of the 4.4-eV dielectric constant for fixed pump-probe time delay. Note that at equal pump fluence the peak in $\text{Im}(\varepsilon)$ and the zero-crossing in $\text{Re}(\varepsilon)$ occur at earlier time delays in the 4.4-eV case than in the 2.2-eV case. Correspondingly, these features occur at lower fluences in the 4.4-eV data than in the 2.2-eV data for equivalent time delays. $\text{Re}(\varepsilon)$ at 4.4 eV crosses zero for fluences as low as 0.5 kJ/m^2 compared to the minimum fluence of 0.8 kJ/m^2 required for a zero-crossing at 2.2 eV.

The behavior of the dielectric constant at 4.4 eV is indeed consistent with the picture described in the previous section of a drop in the average bonding-antibonding splitting. Following the pump pulse excitation, $\Delta E_{b\text{-}a}$ drops from its initial value of about 4.75 eV first past 4.4-eV and then continues down past 2.2-eV. A stronger excitation causes a faster drop through both probe frequencies. At pump fluences between 0.5 kJ/m^2 and 0.8 kJ/m^2, the excitation is strong enough to bring the resonant frequency of the absorption peak below 4.4 eV but not all the way down to 2.2 eV. Note that since 4.4 eV is close to the initial value of the average bonding-antibonding splitting, $\text{Im}[\varepsilon(4.4\text{ eV})]$ does not rise much above its initial value before coming down.

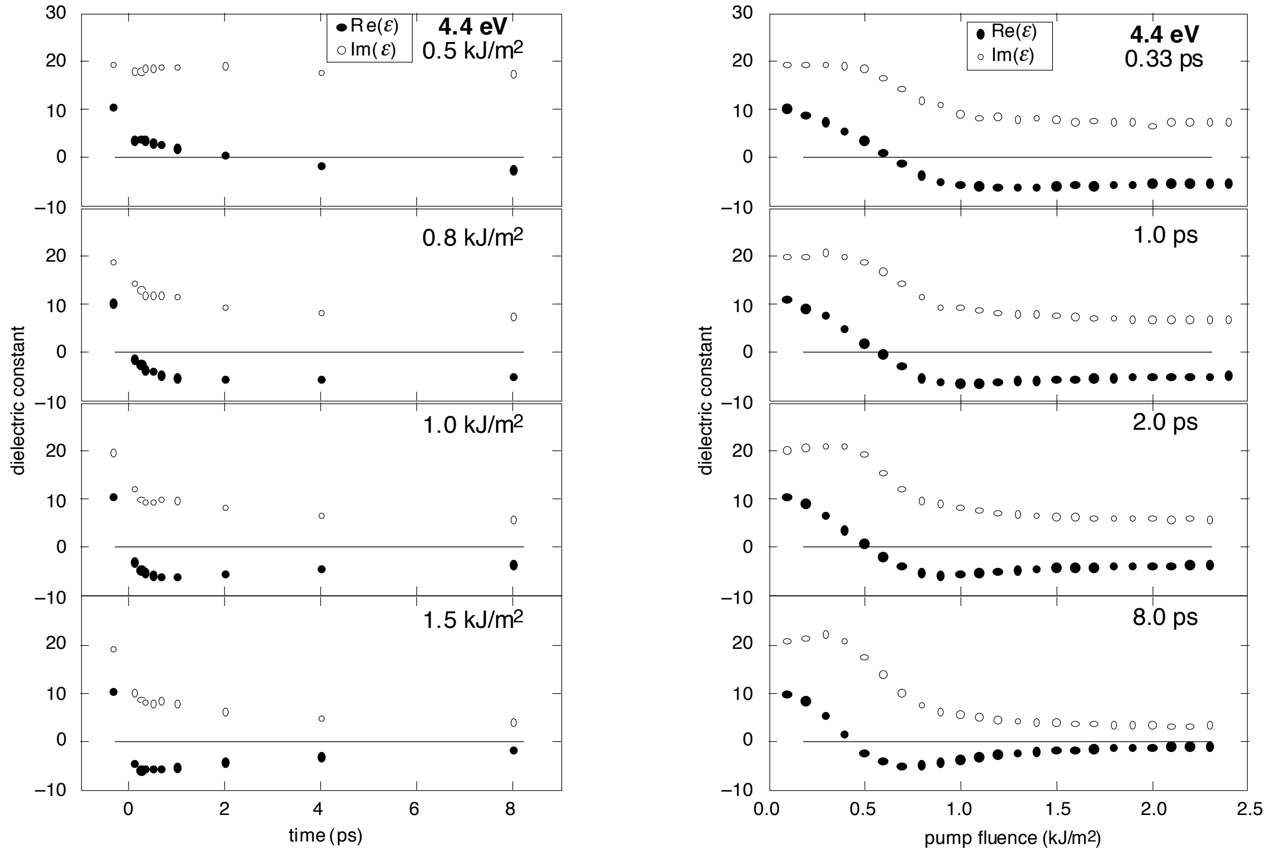

Fig. 6 a, b Dielectric constant at 4.4 eV vs. pump-probe time-delay for four different pump fluences and vs. pump fluence for four different time-delays. ●: Re(ε), ○: Im (ε).

Comparison of Observed Behavior with Expected Behavior

Figure 7 highlights the unexpected nature of the experimental results by comparing the observed behavior of the dielectric constant with that expected based on the basis of the Drude model for the free-carrier contribution. This figure also illustrates the ambiguity inherent in the interpretation of single angle-of-incidence reflectivity measurements. The top graph in Fig. 7a shows the experimentally determined dielectric constant at 2.2 eV plotted against pump fluence at a time delay of 2 ps (this corresponds to the third graph in Fig. 4b). The dielectric constant values in this graph are used to calculate the corresponding *p*-polarized reflectivity at an incident angle of 45°, shown by the curve in the bottom graph in Fig. 7a. This curve agrees with the experimental values of the 45° *p*-reflectivity also measured at a time delay of 2 ps and represented by the open squares in the graph. Fig. 7a therefore provides a consistency check for our two-angle technique. For comparison, Fig. 7b presents in the top graph a Drude-like change in the dielectric constant, without the restriction $\omega\tau \gg 1$, that is chosen to also reproduce the measured 45°-reflectivity values, as seen in the bottom graph. It is important to emphasize that the distinctive resonance features of the actual,

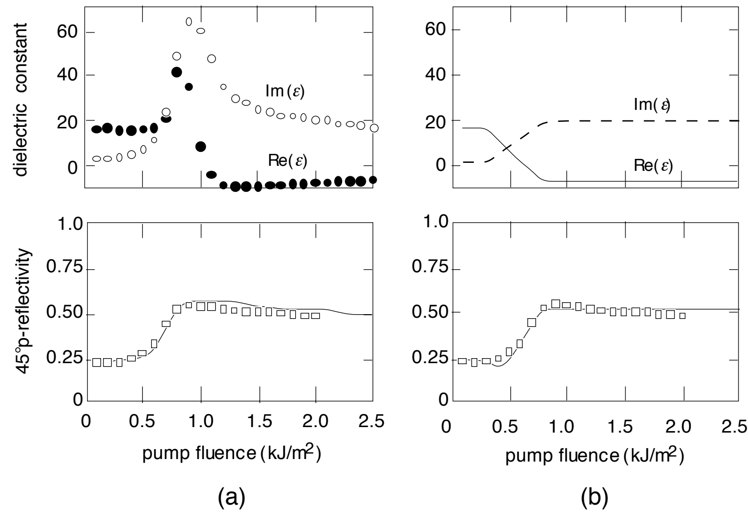

Fig. 7 Comparison of observed behavior with expected behavior at a time delay of 2 ps. (a) Top graph shows experimentally determined values for the 2.2-eV dielectric constant. ●: Re(ε), ○: Im (ε). (b) Top graph shows computer generated, Drude-like dielectric constant chosen to reproduce the measured reflectivity. ———: Re(ε), - - - -: Im(ε). In both (a) and (b), the bottom graph shows the *p*-polarized reflectivity at 45° incident angle. ———: reflectivity calculated from dielectric constant, □: measured reflectivity.

experimentally determined dielectric constant in Fig. 7a produce the same reflectivity values at 45° incidence as the Drude-like behavior of the computer-generated, but incorrect, dielectric constant in Fig. 7b. However, the two dielectric constants reflect very different underlying physics: changes in $\chi_{\text{interband}}(\omega)$ dominate the former while the latter would indicate the prevalence of changes in $\chi_{\text{Drude}}(\omega)$. Thus, experimental determination of the complex dielectric constant is essential to understanding laser-induced phase transitions in semiconductors.

Second-Order Susceptibility

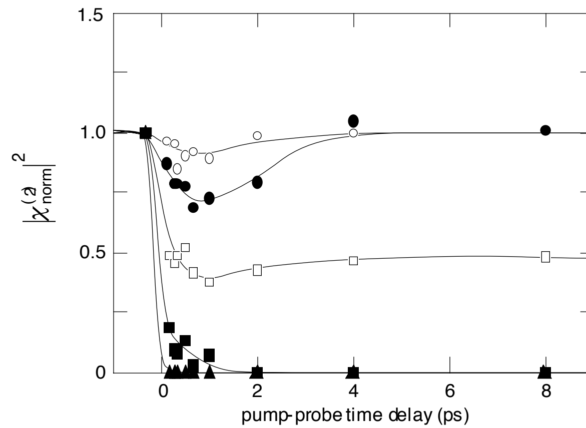

Fig. 8 Square of the second-order susceptibility vs. pump-probe time delay for various pump fluences. The curves are drawn to guide the eye. ○: 0.2 kJ/m^2, ●: 0.4 kJ/m^2, □: 0.6 kJ/m^2, ■: 0.8 kJ/m^2, ▲: 1.5 kJ/m^2.

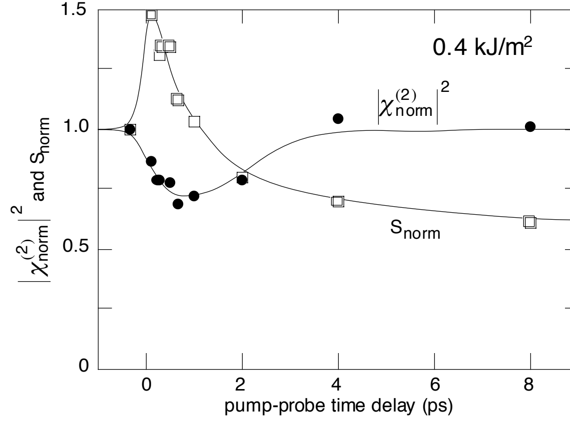

Fig. 9 Normalized second-harmonic signal (□) and square of the second-order susceptibility (●) vs. pump-probe time delay at a pump fluence of 0.4 kJ/m^2. The curves are drawn to guide the eye.

To extract the changes in the second-order susceptibility, we divide the measured second-harmonic signal by the calculated second-harmonic signal based on changes in the linear properties alone. This is described in detail in our previous publication[39]. Figure 8 illustrates the obtained time dependence of $\left|\chi^{(2)}(t)\right|^2$ for various excitation strengths. The results exhibit a range of behaviors, depending on the excitation strength. At pump fluences of 0.8 kJ/m^2 and higher, $\chi^{(2)}$ goes to zero at a rate that increases with pump fluence: at 0.8 kJ/m^2 it takes about 2 ps to reach zero while at 1.5 kJ/m^2 it reaches zero within a pump-probe time delay of 130 fs. In contrast, at pump fluences less than or equal to 0.6 kJ/m^2, $\chi^{(2)}$ undergoes a partial decrease, but it does not reach zero. For pump fluences below 0.5 kJ/m^2, $\chi^{(2)}$ recovers to its initial value on a time scale of a few picoseconds.

At fluences for which $\chi^{(2)}$ does not reach zero, it is particularly important to account for the effects of changes in the dielectric constant on the measured second-harmonic signal. In fact, Fig. 9 shows that the second-harmonic measurements at a fluence of 0.4 kJ/m^2 are actually misleading if one assumes that the behavior of $\left|\chi^{(2)}(t)\right|^2$ is given directly by the second-harmonic signal. Under this assumption, one would conclude from Fig. 9 that at this fluence $\left|\chi^{(2)}(t)\right|^2$ first rises and then drops below its initial value within a few picoseconds. However, our results show that at these fluences $\left|\chi^{(2)}(t)\right|^2$ first *decreases* and then *recovers* to its initial value within a few picoseconds.

Although we focused our attention on the behavior of $\chi^{(2)}$ during the first 10 ps following the excitation, we also measured both the second-harmonic signal and the linear reflectivity at a time delay of a few seconds, after the material has reached its final state. For excitation strengths below 1.0 kJ/m^2, both the second-harmonic signal and the linear reflectivity eventually return to their initial values. However, neither the second-harmonic signal nor the linear reflectivity ever returns to its initial value for pump fluences above 1.0 kJ/m^2. Thus, the changes induced in the material by the laser-pulse excitation are reversible if the pump fluence is

below 1.0 kJ/m^2 but are irreversible if the pump fluence is above 1.0 kJ/m^2. For fluences greater than 0.6 kJ/m^2, once $\chi^{(2)}$ vanishes, it remains zero for at least 100 ps. Thus, the recovery of $\chi^{(2)}$ to its initial value at fluences between 0.6 and 1.0 kJ/m^2 occurs on a time scale which is orders of magnitude larger than the recovery times for fluences less than or equal to 0.5 kJ/m^2.

DISCUSSION

The large changes in the electronic band structure evident in the dielectric constant measurements most likely arise from a combination of electronic screening by the excited free carriers and structural deformation of the lattice resulting from an electronically-induced lattice instability. The free carriers generated by the laser pulse modify the electronic band structure directly through many-body interactions and by screening the ionic potential. A recent calculation shows that these screening effects cause a 2-eV drop in the direct gap at the X-point in GaAs if 10% of the valence electrons are excited to the conduction band — roughly the free-carrier density attained by femtosecond excitation pulses in these experiments[40]. However, the time scale for the drop in the average bonding-antibonding splitting indicates that electronic screening cannot account for the entire bandgap collapse. Screening should be largest immediately following the excitation, *i.e.* when the free-carrier density is highest. As the free-carrier density relaxes through Auger recombination and diffusion, the changes in the electronic band structure due to screening should also relax. Instead, when excited by pulses of about 1.0 kJ/m^2 fluence and less, the average bonding-antibonding splitting continues to drop for picoseconds following the excitation. Thus, while electronic screening is an important effect immediately following the excitation, the changes in the electronic band structure occurring during the first few picoseconds must be due to changes in the lattice structure itself.

The covalent bonds that hold a semiconductor together are only stable if the electrons are in the ground state. Excitation of electrons from bonding valence states to antibonding conduction states breaks the covalent bonds. If enough bonds are broken, the lattice structure will become unstable, *i. e.* certain phonon modes will become soft, and the lattice will begin to deform. Thus, a femtosecond laser pulse can induce a lattice instability if it excites a critical density of electrons, which calculations put at roughly 10% of the valence electrons [41-43]. Under these conditions, the ions can move a significant fraction of the bond length within a few hundred femtoseconds [43, 44]. Since a 10% change in the average bond length is sufficient for the bandgap to collapse [45], this ionic motion can result in a semiconductor-metal transition on a time scale consistent with the experimental data described above.

Note that even below the damage threshold, in the fluence range of 0.8–1.0 kJ/m^2 the laser-pulse excitation induces a drop in the average bonding-antibonding splitting from 4.75 eV down to 2.2 eV within 8 ps. This suggests that reversible structural change takes place below the

permanent damage threshold. The changes in the optical properties are considerably greater than those that could result from lattice heating, even up to the melting temperature of 1511 K. The effect of lattice heating on the dielectric constant has been observed at much lower excitation fluences (10^{-3} kJ/m^2) in Ge and $Si_{1-x}Ge_x$ alloys[13]. Based on the temperature dependence of the optical properties of silicon[46], heating from 10 K up to 1000 K results in about 0.4-eV decrease in the average optical gap. This decrease is linear with temperature above roughly 200 K. Similar temperature dependence has been measured in GaAs, although only up to 300 K, by Walter *et al.*[47] It is quite unlikely that even near the melting temperature the average bonding-antibonding splitting would drop down to 2.2 eV. Finally, the observed resonance in the 0.8–1.0 kJ/m^2 fluence range is very similar to that observed above 1.0 kJ/m^2, only slower, indicating that even below the damage threshold the underlying cause for the drop in the splitting is structural change. The value of 0.8 kJ/m^2 does not represent a fundamental threshold, but is simply the lowest fluence that brings the bonding-antibonding splitting into resonance with the 2.2 eV probe frequency within 8 ps.

Below an excitation fluence of 0.8 kJ/m^2 it is more difficult to identify the source of the observed changes in optical properties. For example, at 0.5 kJ/m^2 excitation (Figure 4a, top graph), we see that the imaginary part of the 2.2 eV dielectric constant has not recovered after 8 ps. Even more pronounced is the drop in the real part of the dielectric constant at 4.4 eV, which also does not recover by 8 ps (Figure 6b, top graph). These persistent effects are due to changes in the bandstructure, and correspond to a downward shift and broadening of the resonant features in the dielectric spectrum. The source of these changes may be lattice heating (thermal motion of the ions), structural change (a deformation of the lattice structure), or a combination of the two.

The interpretation of the behavior of the linear optical properties is complemented by the measurements of the second-order susceptibility. The results presented in the preceding section suggest three main regimes of behavior for $\chi^{(2)}$ following laser-pulse excitation. In the low-fluence regime, below 0.5 kJ/m^2, $\chi^{(2)}$ exhibits a partial drop but recovers to its initial value within a few picoseconds. At medium fluences, from roughly 0.8 to 1.0 kJ/m^2, $\chi^{(2)}$ drops to zero on a time scale between a few hundred femtoseconds and a few picoseconds and remains zero for over 100 ps but eventually also recovers to its initial value. In the high-fluence regime, above 1.0 kJ/m^2, $\chi^{(2)}$ drops to zero within a few hundred femtoseconds and never recovers to its initial value. While a clear boundary at 1.0 kJ/m^2 separates the medium- and high-fluence regimes, no clear boundary separates the low- and medium-fluence regimes. Rather, the behavior gradually changes from low-fluence behavior to medium-fluence behavior between 0.5 kJ/m^2 and 0.8 kJ/m^2.

Structural changes in the lattice most likely dominate the behavior of $\chi^{(2)}$ in the medium- and high-fluence regimes. The time dependence of $\chi^{(2)}$ in these two regimes is not consistent with electronic time scales. First of

all, the recovery time for $\chi^{(2)}$ is greater than 100 ps in the medium-fluence regime compared with electronic relaxation times of a few picoseconds in the low-fluence regime. Moreover, the drop in $\chi^{(2)}$ to zero at fluences greater than 0.6 kJ/m^2 cannot be accounted for by the roughly 10% valence band depopulation achieved by the pump pulse.[48] A structural change in the lattice, however, could lead to a vanishing of $\chi^{(2)}$ on the observed time scales.[43] Recovery times for reversible structural changes should be comparable to lattice relaxation times, which are much greater than 100 ps.[49]

What does the vanishing of $\chi^{(2)}$ imply about the structural changes in the lattice induced by the pump pulse? In the dipole approximation, $\chi^{(2)} = 0$ in materials that have a center of inversion.[20] However, the loss of bulk, dipole $\chi^{(2)}$ does not necessarily mean that the material has taken on a true center of inversion within each unit cell. A loss of long-range order on the scale of the wavelength of light is sufficient to cause such a drop in $\chi^{(2)}$. Experiments show that the degree of amorphization induced by low-dosage ion implantation ($1\times10^{12} - 6\times10^{15}$ cm^{-2} integrated flux of 80-keV Te^+ and S^+ ions) leads to a one-to-two order of magnitude drop in $\chi^{(2)}$.[48] The extent of ionic motion required for GaAs to lose long-range order is much smaller than that required for GaAs to take on a local center of inversion in each unit cell. Given the time scales involved in the data, a loss of long-range order is the most likely explanation for the observed drop in $\chi^{(2)}$ to zero in the medium- and high-fluence regimes.

The $\chi^{(2)}$ data support the conclusion that, for pump fluences greater than 0.6 kJ/m^2, the pump pulse induces an instability in the covalent bonding of GaAs that leads to structural change in the lattice. The instability, which results from the excitation of a critical density of electrons from bonding valence states to antibonding conduction states,[41-43] occurs instantaneously with the generation of free carriers. Because the zincblende structure is no longer stable, the ions start to move away from their ground state positions. As the ions start to move, the material loses its long-range order, and $\chi^{(2)}$ goes to zero. A stronger excitation results in a greater instability and, therefore, faster ionic motion and a faster drop in $\chi^{(2)}$. Below the 1.0 kJ/m^2 threshold, the structural, electronic, and optical changes are reversible.

CONCLUSIONS

Determining the behavior of the optical properties of semiconductors during femtosecond-laser-induced phase transitions provides a window on the complex interplay between the electronic structure and lattice structure of the material. Combining the experimental data on the second-order optical susceptibility with that on the linear optical properties provides a self-consistent picture of the effects of the femtosecond laser-pulse excitation on the semiconductor. The excitation of a critical density of electrons from the valence band to the conduction band destabilizes the covalent bonds in the material. The ionic motion resulting from this laser-induced lattice instability leads to a loss of long-range order in the lattice

structure, evident in the drop to zero of the second-order susceptibility. The deformation of the lattice is accompanied by the drop in the average bonding-antibonding splitting seen in the resonance behavior of the dielectric constant.

ACKNOWLEDGMENTS

We appreciate many useful discussion with Professors N. Bloembergen, H. Ehrenreich, E. Kaxiras, and M. Aziz. E. N. G. gratefully acknowledges a Fannie and John Hertz Fellowship. We would also like to acknowledge financial support from the Joint Services Electronics Program under contract number ONR N00014-89-J-1023 and the National Science Foundation under contract number NSF DMR 89-20490.

REFERENCES

1. C. V. Shank, R. Yen, and C. Hirlimann, Phys. Rev. Lett. **50**, 454 (1983).
2. M. C. Downer, R. L. Fork, and C. V. Shank, J. Opt. Soc. Am. B **2**, 595 (1985).
3. H. W. K. Tom, G. D. Aumiller, and C. H. Brito-Cruz, Phys. Rev. Lett. **60**, 1438 (1988).
4. T. Schröder, W. Rudolph, S. V. Govorkov, and I. L. Shumai, Appl. Phys. A **51**, 1438 (1990).
5. S. V. Govorkov, I. L. Shumay, W. Rudolph, and T. Schroeder, Opt. Lett. **16**, 1013 (1991).
6. K. Sokolowski-Tinten, H. Schulz, J. Bialkowski, and D. von der Linde, Appl Phys A **53**, 227 (1991).
7. P. N. Saeta, J. Wang, Y. Siegal, N. Bloembergen, and E. Mazur, Phys. Rev. Lett. **67**, 1023 (1991).
8. Y. Siegal, E. N. Glezer, and E. Mazur, Phys. Rev. B **49**, 16 (1994).
9. Y. Siegal, E. N. Glezer, L. Huang, and E. Mazur, in *Ultrafast Phenomena in Semiconductors*, edited by D. K. Ferry and H. M. van Driel (SPIE, Bellingham, Washington, 1994).
10. Y. Siegal, E. N. Glezer, and E. Mazur, in *Femtosecond Chemistry*, edited by J. Manz and L. Wöste (Verlag Chemie, Berlin, 1994).
11. E. N. Glezer, Y. Siegal, L. Huang, and E. Mazur, Phys. Rev. B **51**, 6959 (1995).
12. H. Kurz, and N. Bloembergen, in *Energy Beam-Solid Interactions and Transient Thermal Processing*, edited by D. K. Biegelsen, G. A. Rozgonyi and C. V. Shank (Materials Research Society, Pittsburgh, 1985).
13. H. R. Choo, X. F. Hu, and M. C. Downer, Appl. Phys. Lett. **63**, 1507 (1993).
14. X. Y. Wang, and M. C. Downer, Opt. Lett. **17**, 1450 (1992).
15. M. C. Downer, Ahn, Reitze, and X. Y. Wang, Int. J. Thermophysics **14**, 361 (1993).

16. Ahn, X. Y. Wang, and M. C. Downer, in *Short Wavelength V: Physics with Intense Laser Pulses*, edited by M. D. Perry and P. B. Corkum 1993).
17. C. V. Shank, R. Yen, and C. Hirlimann, Phys. Rev. Lett. **51**, 900 (1983).
18. J. M. Liu, A. M. Malvezzi, and N. Bloembergen, in *Energy Beam-Solid Interactions and Transient Thermal Processing*, edited by D. K. Biegelsen, G. A. Rozgonyi and C. V. Shank (Materials Research Society, Pittsburgh, 1985).
19. S. A. Akhmanov, V. I. Emel'yanov, N. I. Koroteev, and V. N. Seminogov, Sov Phys Usp **28**, 1084 (1985).
20. Y. R. Shen, *The Principles of Nonlinear Optics*; (John Wiley & Sons, New York, 1984).
21. M. L. Cohen, and J. R. Chelikowsky, *Electronic Structure and Optical Properties of Semiconductors*; (Springer-Verlag, Berlin, 1988).
22. W. A. Harrison, *Electronic Structure and the Properties of Solids: The Physics of the Chemical Bond*; (Dover, New York, 1989).
23. H. R. Philipp, and H. Ehrenreich, Phys. Rev. **129**, 1550 (1963).
24. E. D. Palik, in *Handbook of Optical Constants of Solids*, edited by E. D. Palik (Academic Press, Inc., New York, 1985).
25. D. E. Aspnes, G. P. Schwartz, G. J. Gualtieri, A. A. Studna, and B. Schwartz, J. Electrochem. Soc. **128**, 590 (1981).
26. J. D. Jackson, *Classical Electrodynamics*; (Wiley, New York, 1975).
27. A. M. Malvezzi, H. Kurz, and N. Bloembergen, in *Energy Beam-Solid Interactions and Transient Thermal Processing*, edited by D. K. Biegelsen, G. A. Rozgonyi and C. V. Shank (Materials Research Society, Pittsburgh, 1985).
28. P. N. Saeta, Ph.D. Thesis, Harvard University, 1991.
29. A. Othonos, H. M. van Driel, J. F. Young, and P. J. Kelly, Solid-State Electron. **32**, 1573 (1989).
30. P. M. Fauchet, and K. D. Li, J. Non-Crystalline Solids **97&98**, 1267 (1987).
31. H. M. van Driel, Phys Rev B **35**, 8166 (1987).
32. A. Othonos, H. M. van Driel, J. F. Young, and P. J. Kelly, Phys. Rev. B **43**, 6682 (1991).
33. J. K. Wang, Y. Siegal, C. Z. Lü, and E. Mazur, Opt. Comm. **91**, 77 (1992).
34. Y. Siegal, Ph.D. Thesis, Harvard University, 1994.
35. Note that if the oscillator strength and the spectral width of an absorption peak are held fixed, then the height of the absorption peak increases as its resonant frequency decreases.
36. D. L. Greenaway, and G. Harbeke, *Optical Properties and Band Structure of Semiconductors*; (Pergamon Press, Oxford, 1968).
37. R. F. Potter, in *Optical Properties of Solids*, edited by S. Nudelman and S. S. Mitra (Plenum Press, New York, 1969).
38. D. H. Reitze, H. Ahn, and M. C. Downer, Phys. Rev. B **45**, 2677 (1992).

39. E. N. Glezer, Y. Siegal, L. Huang, and E. Mazur, Phys. Rev. B **51**, 9589 (1995).
40. D. H. Kim, H. Ehrenreich, and E. Runge, Solid State Commun. **89**, 119 (1994).
41. J. A. Van Vechten, R. Tsu, and F. W. Saris, Phys. Lett. **74A**, 422 (1979).
42. R. Biswas, and V. Ambegoakar, Phys. Rev. B **26**, 1980 (1982).
43. P. Stampfli, and K. H. Bennemann, Phys. Rev. B **42**, 7163 (1990).
44. P. Stampfli, and K. H. Bennemann, J. Phys. Condens. Matter **5**, supplement, A173 (1993).
45. S. Froyen, and M. L. Cohen, Phys. Rev. B **28**, 3258 (1983).
46. G. E. Jellison, and F. A. Modine, Phys. Rev. B **27**, 7466 (1983).
47. J. P. Walter, R. R. L. Zucca, M. L. Cohen, and Y. R. Shen, Phys. Rev. Lett. **24**, 102 (1970).
48. S. A. Akhmanov, M. F. Galyautdinov, N. I. Koroteev, G. A. Paityan, I. B. Khaibullin, E. I. Shtyrkov, and I. L. Shumai, Bull. Acad. Sci. USSR, Phys. Ser. **49**, 86 (1985).
49. F. Spaepen, in *Ultrafast Phenomena V*, edited by G. R. Fleming and A. E. Siegman (Springer-Verlag, Berlin, 1986).